Lepton-proton two-photon exchange in chiral perturbation theory

Pulak Talukdar[1,*], Vanamali C. Shastry[2,†], Udit Raha,[1,‡] and Fred Myhrer[3,§]

[1]*Department of Physics, Indian Institute of Technology Guwahati, Guwahati-781039, Assam, India*
[2]*Department of Education in Science and Mathematics,*
Regional Institute of Education Mysuru, Mysore-570006, India
[3]*Department of Physics and Astronomy, University of South Carolina,*
Columbia, South Carolina 29208, USA

We use heavy baryon chiral perturbation theory to evaluate the two-photon exchange corrections to the low-energy elastic lepton-proton scattering at next-to-leading order accuracy, i.e., $\mathcal{O}(\alpha, M^{-1})$, including a nonzero lepton mass. We consider the elastic proton intermediate state in the two-photon exchange invoking soft photon approximation. The infrared singular contributions are projected out using dimensional regularization. The resulting infrared singularity-free two-photon exchange contribution is in good numerical agreement with existing predictions based on standard diagrammatic soft photon approximation evaluations.

I. INTRODUCTION

During the past few decades electron-proton (ep) scattering experiments at various experimental facilities, e.g., BINP Novosibirsk, SLAC, DESY, Fermilab, CERN, JLab, and MAMI, have provided great insights into the electromagnetic structure of the proton. The pointlike nature of the electrons as well as the small value of the electromagnetic coupling make them ideal probes for investigating the internal structure of the proton. Polarized and unpolarized cross section measurements with ultrarelativistic electrons have yielded information on physical quantities, such as electromagnetic form factors, parton distribution functions, and polarization asymmetries. However, in recent years the values of some low-energy physical quantities extracted from such experiments show discrepancies which are currently difficult to reconcile. The most contentious being the measurements of the *root-mean-square* (rms) proton radius extracted from ep scattering data versus the ones from the CREMA Collaboration measurements, which are high-precision muonic hydrogen Lamb-shift determinations, leading to about 5σ discrepancy with the previous accepted proton rms value [1–7]. We note that a very recent hydrogen Lamb-shift measurement [8], however, reported a result consistent with the CREMA measurement [1,2]. This so-called "proton radius puzzle," together with the well-known discrepancy of the electric to magnetic form factor ratio (G_E/G_M) of the proton [9–17], has resulted

in a renewed vigor in the study of the structure of the proton both experimentally and theoretically (see, e.g., Refs. [4,18–20] for recent reviews).

The proton rms radius is determined from the proton's electric form factor (G_E) which may be obtained from the measurement of the unpolarized elastic lepton-proton (ℓp) scattering cross section. The rms electric charge radius ($\sqrt{\langle r_E^2 \rangle}$) is thereby extracted using the relation $\langle r_E^2 \rangle = 6 \frac{\partial G_E(Q^2)}{\partial Q^2}\big|_{Q^2=0}$ where, Q^2 is the four-momentum transfer. One of the challenges associated with the measurements of the ℓp cross section at low-energy or low-Q^2 values is the bremsstrahlung process, $\ell p \rightarrow \ell p \gamma$, which constitutes an important background. The data analysis entails the disentanglement of this background from the elastic ℓp scattering process before the rms radius can be extracted. To yield meaningful results one needs to deal with the *soft* photon emissions, leading to infrared (IR) divergences that must cancel with the IR-divergent virtual photon exchange counterparts. This so-called *unfolding procedure* of the radiative analysis of the *raw* data [21–25] makes an experimental determination of the rms radius rather intricate especially at low energies.

Several recent experimental proposals, including low-energy ℓp scattering experiments, are under way to resolve the rms discrepancy. For example, the Prad [26,27] experiment at JLab and the MUon proton Scattering Experiment (MUSE) [28,29] at PSI are two such experiments. In particular, the MUSE Collaboration aims to measure the elastic $\mu^\pm p$ scattering cross sections at momentum transfer as low as $|Q^2| \sim 0.002$–0.08 GeV/c^2 [28,29]. In fact, MUSE plans to extract the proton's rms radius from very precise

---
[*]t.pulak@iitg.ac.in
[†]vanamalishastry@gmail.com
[‡]udit.raha@iitg.ac.in
[§]myhrer@mailbox.sc.edu

measurements (with a projected accuracy of less than 1%) of the $\mu^{\pm}p$ and $e^{\pm}p$ cross sections. This should facilitate a comparative study of the extracted rms radii from these low-energy elastic scattering processes under very similar experimental conditions.

The proton is an extended particle composed of quarks and gluons, and for low-energy probes one is faced with complexities arising from the underlying nonperturbative nature of strong interactions. This low-energy theory is usually parametrized; the proton-photon vertices are described by electric and magnetic (Sachs) form factors. The form factors are either phenomenologically modeled, extracted directly from experimental data, or determined via *ab initio* numerical calculations using lattice QCD. Well-known works from the past [21–23], as well as many recent works in the past two decades (e.g., [18–20,30,31] and other references therein) on radiative correction analyses, relied on such phenomenological form factors. In contrast, our analysis presented in this work makes use of elementary pointlike vertices derived in the context of an *effective field theory* (EFT). The work of Tsai [21] presented a detailed account of the radiative correction analysis for the elastic electron-proton scattering process where the relativistic recoil corrections for the proton were considered. This analysis therefore predominantly concentrated on the high-energy regime of the lepton scattering process. In a later work, Mo and Tsai [22] introduced the so-called *peaking approximation* which is justifiable for electron scattering off the proton even at low energies, as confirmed in, e.g., Refs. [32,33].

One of the earliest works on the *two-photon exchange* (TPE) effects may be the so-called *Feshbach corrections* [34], which considered relativistic electrons scattering off a static Coulomb potential. The later works of Refs. [21–23] did consider the virtual TPE diagrams in order to cancel the IR divergences arising from the bremsstrahlung diagrams. These calculations suggested that the TPE effects were small. In other words, the dominant contributions arose from the *one-photon exchange* contribution (i.e., the first Born approximation) leading to the celebrated Rosenbluth formula for elastic lepton-proton scattering cross section. Modern experimental arrangements such as the MUSE facilitate simultaneous measurement of the unpolarized elastic $e^{\pm}p$ and $\mu^{\pm}p$ scattering cross sections, thereby enabling the extraction of possible enhanced TPE contributions. In other words, MUSE will measure the difference of the lepton and antilepton charge cross sections to which the interference between the Born and the TPE diagrams at $\mathcal{O}(\alpha^3)$ contributes.[1]

Recent theoretical studies have suggested that the TPE effects can play a crucial role in explaining possible discrepancies in various measured observables. It appears to be the general consensus that the TPE contributions have the correct sign and magnitude in order to resolve the bulk of the discrepancies in the extraction of form factors [4,9–19]. This brought about a renaissance in TPE studies relating to the ℓp scattering process. A wide variety of hadronic model analyses of the TPE contributions include dispersion theory methods [35–49],[2] resonance exchange models, and dynamical coupled channel K-matrix analyses [50–55]. In these evaluations of the TPE processes, inelastic intermediate states of the nucleon and the Δ, namely, the N^*, Δ^*, and other possible excitation, along with various resonance exchanges, such as σ, ω, ϕ, were considered which could contribute even at small momentum transfers, $|Q^2| \lesssim 0.1 \ (\mathrm{GeV}/c)^2$ [19]. Contributions from these intermediate excited states are expected to be small at such low $|Q^2|$. Moreover, there has been a report of an interesting interplay between the spin-1/2 and spin-3/2 resonance states leading to partial cancellations among the above excited states of nucleon and Δ contributions to the TPE [53]. Ultimately, the TPE with the elastic proton intermediate state is expected to give the dominant contribution at very low momentum transfers [30, 45–47,49,56,57]. In this work we focus only on the intermediate elastic proton contributions to the TPE diagrams. Furthermore, here we only need to deal with the real parts of these amplitudes which contribute to the unpolarized elastic lepton-proton cross section.

As already mentioned, the TPE contributions contain IR divergences which are canceled by the IR terms arising from the soft photon bremsstrahlung process at $\mathcal{O}(\alpha^3)$. In this work, we present an evaluation of TPE contributions with a proton intermediate state using a low-energy EFT, namely the heavy baryon chiral perturbation theory (HBχPT), which is an effective low-energy field theory of QCD (e.g., [58,59] and references therein). The primary motivation for the use of HBχPT is to provide a systematic, model independent evaluation of the TPE intermediate proton contribution at low energies incorporating simultaneous radiative and proton recoil effects. HBχPT entails a perturbative expansion of the chiral Lagrangian based on a momentum expansion scheme. The *leading chiral order* (LO) terms give the dominant amplitudes, and the *next-to-leading order* (NLO) amplitudes normally, viz., in a naive dimensional analysis, are smaller corrections to the LO amplitudes of the process. HBχPT also includes a well established perturbative counting expansion in inverse powers of the nucleon mass M consistent with the chiral momentum expansion. Since the chiral symmetry

---

[1]These *charge-asymmetry* measurements cannot be used to extract the TPE contribution directly. The MUSE experiment can instead observe the *charge odd* combinations of TPE along with parts of the bremsstrahlung contributions. In order to isolate the TPE contribution, model-dependent corrections must be applied to the charge-asymmetry data; i.e., one has to extract the charge-dependent bremsstrahlung contributions, e.g., Ref. [19].

[2]*En passant*, Refs. [41,42] used dispersion relations to predict a smaller value of the proton's charge radius ~0.84–0.85 fm, prior to the CREMA muonic hydrogen measurements [1,2].

breakdown scale Λ_χ is of the order of $M \sim 1$ GeV, the expansion parameter, $Q/\Lambda_\chi \sim m_\pi/\Lambda_\chi \ll 1$, includes both the chiral expansion and the expansion in M^{-1}. Moreover, the electromagnetic interaction naturally enters HBχPT in a gauge invariant way.

Thus, HBχPT provides the ideal framework to study low-energy processes such as the ℓp scattering, where nucleons, mesons, and leptons are the fundamental degrees of freedom. Especially in dealing with MUSE-like kinematics where the lepton mass plays a sensitive role, the widely used ultrarelativistic approximation of leptons cannot be employed [32,33]. At such low-Q^2 processes, the predictive power of HBχPT becomes very effective. Furthermore, the power counting of HBχPT allows a systematic control of the uncertainties involved. These uncertainties could be improved order-by-order in the expansion scheme of HBχPT. This nonrelativistic field theory has been used extensively in the past to study the physical properties and the low-energy dynamics of nucleons and other baryons [58,59]. In this work we use the same framework to analytically evaluate the TPE *box* and *cross-box* diagrams (called *TPE box* hereafter) and the so-called *seagull* diagram (cf. Fig. 1.) While all the TPE box diagrams are ultraviolet (UV) finite, the seagull diagram is both IR as well as UV finite. In this work we shall use the
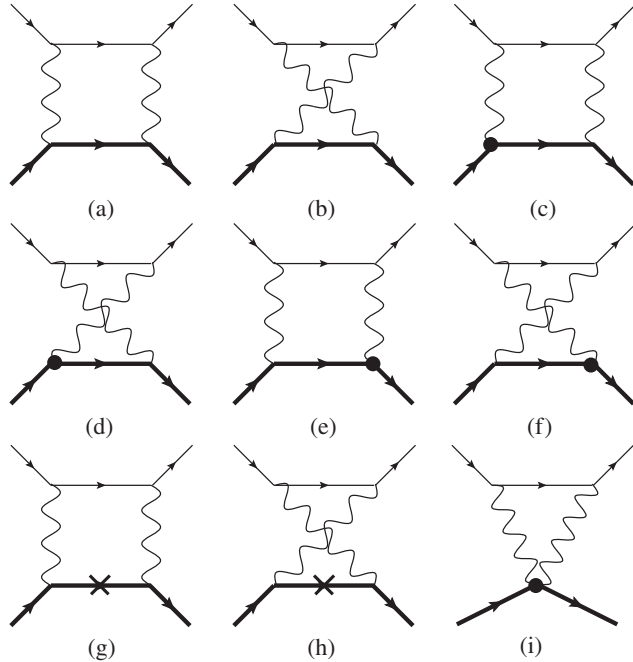

FIG. 1. The TPE Feynman diagrams of $\mathcal{O}(e^4)$ which contribute to the $\mathcal{O}(\alpha^3)$ interference term in the elastic lepton-proton cross section. Thin lines represent lepton propagators, thick lines represent proton propagators, and wiggly lines represent photon propagators. The solid dark circles and the lines with a cross represent vertex and proton propagator insertions, respectively, from the NLO Lagrangian $\mathcal{L}_{\pi N}^{(1)}$. Diagrams (a)–(h) are the "box" and "cross-box" terms, and diagram (i) is the "seagull" term.

gauge invariance-preserving dimensional regularization (DR) scheme in order to remove the IR singularities from the TPE box diagrams. To the best of our knowledge such a TPE evaluation in the context of HBχPT has not been pursued until now.

The paper is organized as follows. In Sec. II we introduce the general formalism for elastic lepton-proton scattering within HBχPT, providing the relevant terms from the chiral Lagrangian, *up-to-and-including* NLO in the chiral power counting, that is necessary for the evaluation of our TPE diagrams. We also discuss some of the details of the kinematics involved in the calculations, which are commensurate with the proposed MUSE kinematic domain. In Sec. III, we outline the crucial steps involved in the systematic removal of the IR divergences from the TPE diagrams at $\mathcal{O}(\alpha^3)$. Especially, we discuss the subtle nature of many cancellations among the NLO TPE amplitudes in the soft photon limit and their relation to the corresponding soft photon bremsstrahlung processes. Next in Sec. IV we present our numerical estimates of the TPE contribution to the unpolarized elastic cross section. Finally in Sec. V we draw some conclusions and present our outlook. Appendix is included at the end which collects some of the details of our analytical evaluation of the seagull diagram.

II. HEAVY BARYON CHIRAL PERTURBATION THEORY TREATMENT OF LEPTON-PROTON SCATTERING

The relevant parts of the LO and NLO chiral Lagrangian needed in our TPE evaluation of the lepton proton scattering amplitudes are given in, e.g., Ref. [58]. Since at NLO the TPE vertices do not involve pions, we ignore the pion degrees of freedom in the part of the chiral Lagrangian that we use [the pion loops arise at *next-to-next-to-leading order* (NNLO) which is beyond the accuracy of this work.] From Ref. [58] we obtain

$$\mathcal{L}_N = \mathcal{L}_N^{(\nu=0)} + \mathcal{L}_N^{(\nu=1)} + \cdots, \tag{1}$$

where the chiral indices $\nu = 0$ and $\nu = 1$ represent the LO and NLO components of the HBχPT Lagrangian[3]

$$\mathcal{L}_N^{(0)} = \bar{N}(iv \cdot D + g_A S \cdot u)N, \tag{2}$$

$$\mathcal{L}_{\pi N}^{(1)} = \bar{N}\left\{\frac{1}{2M}(v \cdot D)^2 - \frac{1}{2M}D \cdot D + \cdots\right\}N. \tag{3}$$

Here $N = (\text{p} \ \text{n})^{\text{T}}$ is the heavy nucleon spin-isospin field, and v_μ and S_μ are the nucleon velocity and spin four-vectors satisfying the condition $v \cdot S = 0$. Here we choose

---

[3]Ideally M is the mass of the nucleon in the chiral limit. In this work we use M also to denote the proton's physical mass, $M = 938.28$ MeV.

$v = (1, \mathbf{0})$ such that $S = (0, \boldsymbol{\sigma}/2)$. The covariant derivatives in the Lagrangian are

$$D_\mu = \partial_\mu + \Gamma_\mu - i v_\mu^{(s)}, \qquad u_\mu = i u^\dagger \nabla_\mu U u^\dagger, \quad (4)$$

$$\Gamma_\mu = \frac{1}{2}[u^\dagger(\partial_\mu - i r_\mu)u + u(\partial_\mu - i l_\mu)u^\dagger], \quad (5)$$

$$\nabla_\mu U = \partial_\mu U - i r_\mu U + i U l_\mu. \quad (6)$$

Due to the absence of the explicit pions the $u = \sqrt{U}$ field is simply $u = I \equiv I_{2\times2}$, the identity matrix in isospin space. The external isovector right and left fields, r_μ and l_μ, respectively, have in our case simple expressions since the only external source field is the photon field $A_\mu(x)$. The chiral Lagrangian is therefore reduced to a combination of external isoscalar source $v_\mu^{(s)} = -e\frac{I}{2}A_\mu(x)$ and isovector source $u_\mu = (l_\mu + r_\mu)/2 = -e\frac{\tau^3}{2}A_\mu(x)$, where τ^3 is the third Pauli isospin matrix.

The relevant TPE amplitudes of $\mathcal{O}(e^4)$ are diagrammatically illustrated in Fig. 1. In the diagrams labeled (a) and (b), the proton-photon vertices arise from the LO chiral Lagrangian, while diagrams (c)–(f) contain one proton-photon vertex insertion from the NLO Lagrangian. Each of the diagrams (g) and (h) contains an NLO propagator insertion, and finally the seagull diagram (i) contains no intermediate proton; instead this diagram has an effective two-photon interaction vertex associated with the proton originating from the NLO Lagrangian.

In this work we find it convenient to use the laboratory or rest frame of the proton target which allows a straight-forward relation to the proposed MUSE kinematic. The convention used here is shown in Fig. 2, where the incoming lepton momentum $p = (E, \mathbf{p})$, the outgoing lepton momentum $p' = (E', \mathbf{p}')$, the incoming proton momentum $P = (M, \mathbf{0})$, and the outgoing proton momentum $P' = (E'_p, \mathbf{P}')$. Additionally, in the HBχPT formalism one introduces a small so-called *residual* incoming proton momentum p_p as defined through the relation
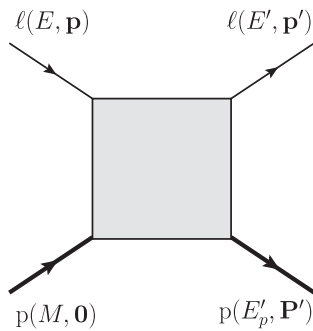

FIG. 2. The kinematics for the $\ell p \to \ell p$ scattering in the laboratory frame. The square shaded area represents all possible internal graphs contributing to the elastic scattering process.

TABLE I. The MUSE range of $|Q^2|$ values for ep and μp scattering at the two limits of the laboratory frame scattering angle, namely, $\theta = 20°$ and $100°$, obtained from Eq. (8).

Momentum (p) in GeV/c	0.115	0.153	0.210
$|Q^2|$ in (GeV/c)^2 for electron			
Angle $\theta = 20°$	0.0016	0.0028	0.0052
Angle $\theta = 100°$	0.027	0.046	0.082
$|Q^2|$ in (GeV/c)^2 for muon			
Angle $\theta = 20°$	0.0016	0.0028	0.0052
Angle $\theta = 100°$	0.026	0.045	0.080

$P^\mu = M v^\mu + p_p^\mu$ with $p_p^2 \ll M^2$, which in the laboratory frame means $v \cdot p_p = 0$. Similarly, the small residual outgoing proton momentum p'_p defined as $P'^\mu = M v^\mu + p'_p{}^\mu$, where $(p'_p)^2 \ll M^2$, implies

$$v \cdot p'_p = \frac{\mathbf{p}'^2_\mathbf{p}}{2M} + \mathcal{O}(M^{-2}). \quad (7)$$

Finally, the four-momentum transfer in the elastic process is $Q_\mu = p_\mu - p'_\mu = P'_\mu - P_\mu = (p'_p)_\mu - (p_p)_\mu$, and the lepton scattering angle is θ.

The MUSE Collaboration has chosen the incident lepton momenta to have the following values: 115 MeV/c, 153 MeV/c, and 210 MeV/c. This means that for elastic scattering the four-momentum transfer Q^2 depends only on the scattering angle θ. The corresponding range of the Q^2 value in the laboratory frame can be obtained using the relations

$$Q^2 = 2m_l^2 - 2EE'(1 - \beta\beta'\cos\theta) = -2M(E - E'), \quad (8)$$

where $\beta = |\mathbf{p}|/E$ and $\beta' = |\mathbf{p}'|/E'$ are the incoming and outgoing lepton velocities, respectively. It may be shown that $0 < |Q^2| < |Q^2_{\max}| = 4M^2(E^2 - m_l^2)/(m_l^2 + M^2 + 2ME)$ represents the kinematically allowed (physical) range of momentum transfers [30]. However, the (laboratory frame) scattering angle is proposed by MUSE to be in the range $\theta \in [20°, 100°]$ [28], for which the possible Q^2 range of values obtained from Eq. (8) are tabulated in Table I. By examining the Q^2 values in the table we observe that $Q/\Lambda_\chi \ll 1$; i.e., the HBχPT power counting scheme can be applied reasonably well in the domain of the MUSE kinematics.[4] Here we remark that the lepton mass is explicitly included in all our expressions. In the next section we evaluate the TPE diagrams in Fig. 1 and isolate the IR divergences of the TPE box diagrams.

---

[4]We note that for the TPE diagrams with either NLO vertex or propagator insertions being already of $\mathcal{O}(M^{-1})$, it is reasonable to write $E' = E + \frac{Q^2}{2M} \approx E$ at NLO.

III. TWO-PHOTON EXCHANGE IN THE SOFT PHOTON APPROXIMATION

In this section we evaluate all the TPE diagrams in Fig. 1 using HBχPT and derive the Q^2 or θ dependence on the IR subtracted TPE diagrams in a gauge-invariant manner. The finite (IR subtracted) part of the TPE fractional corrections $\bar{\delta}_{\gamma\gamma}$ up to and including next-to-leading order accuracy, i.e., $\mathcal{O}(\alpha, M^{-1})$, to the elastic scattering cross section is defined by

$$\left[\frac{d\sigma_{el}(Q^2)}{d\Omega_l'}\right]_{\gamma\gamma} = \left[\frac{d\sigma_{el}(Q^2)}{d\Omega_l'}\right]_{\gamma} \bar{\delta}_{\gamma\gamma}(Q^2), \qquad (9)$$

where

$$\bar{\delta}_{\gamma\gamma}(Q^2) = \frac{2\mathcal{R}e\sum_{\text{spins}}(\mathcal{M}_{\gamma}^*\mathcal{M}_{\gamma\gamma})}{\sum_{\text{spins}}|\mathcal{M}_{\gamma}|^2} - \delta_{\text{IR}}^{(\text{box})}(Q^2). \qquad (10)$$

In this expression $\mathcal{M}_\gamma$ is the one-photon exchange (Born) amplitude,

$$\mathcal{M}_\gamma = -\frac{e^2}{Q^2}[\bar{u}(p')\gamma^\mu u(p)][\chi^\dagger(p_p')v_\mu\chi(p_p)], \quad (11)$$

and $\mathcal{M}_{\gamma\gamma} = \mathcal{M}_{\gamma\gamma}^{(\text{box})} + \mathcal{M}_{\text{seagull}}^{(i)}$ is the total TPE amplitude obtained by summing the TPE box amplitudes, $\mathcal{M}_{\gamma\gamma}^{(\text{box})}$, and the seagull amplitude, $\mathcal{M}_{\text{seagull}}^{(i)}$, viz., Feynman diagrams (a)–(i) in Fig. 1. The corresponding Born cross section is $(d\sigma_{el}/d\Omega_l')_\gamma$, which to LO in the chiral expansion (including phase space $1/M$ proton recoil contributions) is given by

$$\left[\frac{d\sigma_{el}(Q^2)}{d\Omega_l'}\right]_\gamma = \frac{1}{64\pi^2 M^2}\left(\frac{\beta' E'}{E}\right)\left[1 + \frac{E}{M}(1-\cos\theta)\right]^{-1}$$
$$\times \frac{1}{4}\sum_{\text{spins}}|\mathcal{M}_\gamma|^2,$$

$$\frac{1}{4}\sum_{\text{spins}}|\mathcal{M}_\gamma|^2 = \frac{64\pi^2\alpha^2}{Q^4}MEE'(M+E_p')$$
$$\times\left[1 + \beta\beta'\cos\theta + \frac{m_l^2}{EE'}\right], \qquad (12)$$

where the kinematics at $1/M$ order accuracy yield the following relations:

$$E' = E\left[1 - \frac{\beta^2 E}{M}(1-\cos\theta) + \mathcal{O}(M^{-2})\right],$$

$$\beta' = \beta\left[1 - \frac{(1-\beta^2)E}{M}(1-\cos\theta) + \mathcal{O}(M^{-2})\right],$$

$$Q^2 = -2\beta^2 E^2(1-\cos\theta)$$
$$\times\left[1 - \frac{E}{M}(1-\cos\theta) + \mathcal{O}(M^{-2})\right]. \qquad (13)$$

In Eq. (10), the term $\delta_{\text{IR}}^{(\text{box})}$ denotes the IR singular part of the TPE box diagrams' contribution to the elastic cross section. Utilizing DR we project out these singularities before deriving the expression for $\delta_{\text{IR}}^{(\text{box})}$. It will be shown in a future publication [60] that the $\mathcal{O}(e^3)$ soft bremsstrahlung amplitude has an IR singularity which in the cross section generates a singular term, $\delta_{\text{IR}}^{(\text{soft})}$, which cancels the IR singularity in Eq. (10), namely, $\delta_{\text{IR}}^{(\text{soft})} = -\delta_{\text{IR}}^{(\text{box})}$ at $\mathcal{O}(\alpha^3)$. Our calculations of the finite TPE contribution $\bar{\delta}_{\gamma\gamma}$ in Eq. (10) inherently rely on the widely used *soft photon approximation* (SPA). While the HBχPT evaluation details and discussion of the full QED radiative corrections to the ℓp elastic scattering at NLO will be presented in Ref. [60], here we simply quote our analytical expression for $\delta_{\text{IR}}^{(\text{soft})}$:

$$\delta_{\text{IR}}^{(\text{soft})}(Q^2) = \frac{\alpha Q^2}{2\pi ME}\left\{\frac{1}{\epsilon} - \gamma_E + \ln\left(\frac{4\pi\mu^2}{-Q^2}\right)\right\}$$
$$\times\left\{\frac{1}{\beta}\ln\sqrt{\frac{1+\beta}{1-\beta}} + \frac{E}{E'\beta'}\ln\sqrt{\frac{1+\beta'}{1-\beta'}}\right\}. \qquad (14)$$

The TPE diagrams in Fig. 1 naturally include the contributions to the Coulomb wave functions describing the incoming and outgoing charged leptons. For example, the so-called "Coulomb focusing" or distortion of the scattered lepton spectrum at low-$|Q^2|$ is explained by considering one of the exchanged photons in the box diagrams as a soft photon.[5] The SPA has widely been used in the literature as a practical tool to isolate the IR singularities of the TPE box diagrams. However, the exact implementation of the SPA is somewhat *ad hoc* and differs in different theoretical works. For example, following the work of Maximon and Tjon [23], the SPA is used only in

---

[5]The Coulomb distortion of the outgoing electron waves in the second Born approximation was investigated in Refs. [61,62] (see also Figs. 13 and 17 of Ref. [19]) where it was found to significantly enhance the cross section at backward scattering angles. However, in this case the contribution to the proton's rms charge radius is unlikely to be affected from the extrapolation of the form factor data to extreme forward angles where Coulomb wave function effects are found to be small. Hence, the authors of Refs. [61,62] concluded that the radius discrepancy could not have been attributed to an erroneous experimental measurement due to the influence of this kind of SPA in the TPE contributions.

the denominator (propagators) of the integrand in order to single out the IR-divergent TPE amplitude; i.e., the momentum of the soft exchange photon is set to zero. Maximon and Tjon do not set the photon momentum to zero in the numerator of the integrand. On the other hand, following the work of Mo and Tsai [22], the SPA is used simultaneously in the numerator and denominator. As was noted in Ref. [23], the convenience of using the former "less drastic" type of approximation is that the resulting expressions become somewhat simpler. However, some authors, e.g., those of Ref. [57], have argued in favor of the latter "more drastic" approximation being more self-consistent.

The essential point is to let the momenta associated with the soft photon go to zero, irrespective of whether they appear in the numerator or the denominator. Since these soft momentum factors, which appear in the numerator of the amplitudes, originate from those in the denominator, it seems somewhat unreasonable to let them go to zero *only* in the denominator. Concurring with the argument presented in Ref. [57], in the following we shall use the SPA definition of Mo and Tsai [22].

As shown in Figs. 1(a)–1(i), the loop integrals up to NLO in HBχPT contributing to the TPE amplitude $\mathcal{M}_{\gamma\gamma}$ are, respectively, given by

$$i\mathcal{M}_{\text{box}}^{(a)} = e^4 \int \frac{d^4k}{(2\pi)^4} \frac{[\bar{u}(p')\gamma^\mu(\not{p}-\not{k}+m_l)\gamma^\nu u(p)][\chi^\dagger(p'_p)v_\mu v_\nu \chi(p_p)]}{(k^2+i0)[(Q-k)^2+i0](k^2-2k\cdot p+i0)(v\cdot k+i0)}, \tag{15}$$

$$i\mathcal{M}_{\text{xbox}}^{(b)} = e^4 \int \frac{d^4k}{(2\pi)^4} \frac{[\bar{u}(p')\gamma^\mu(\not{p}-\not{k}+m_l)\gamma^\nu u(p)][\chi^\dagger(p'_p)v_\mu v_\nu \chi(p_p)]}{(k^2+i0)[(Q-k)^2+i0](k^2-2k\cdot p+i0)(-v\cdot k+i0)}, \tag{16}$$

$$i\mathcal{M}_{\text{box}}^{(c)} = \frac{e^4}{2M} \int \frac{d^4k}{(2\pi)^4} \frac{[\bar{u}(p')\gamma^\mu(\not{p}-\not{k}+m_l)\gamma^\nu u(p)][\chi^\dagger(p'_p)\{v_\mu(2p_p+k)_\nu - v_\mu v_\nu(v\cdot k)\}\chi(p_p)]}{(k^2+i0)[(Q-k)^2+i0](k^2-2k\cdot p+i0)(v\cdot k+i0)}, \tag{17}$$

$$i\mathcal{M}_{\text{xbox}}^{(d)} = \frac{e^4}{2M} \int \frac{d^4k}{(2\pi)^4} \frac{[\bar{u}(p')\gamma^\mu(\not{p}-\not{k}+m_l)\gamma^\nu u(p)][\chi^\dagger(p'_p)\{v_\nu(p_p+p'_p-k)_\mu - v_\mu v_\nu(-v\cdot k))\}\chi(p_p)]}{(k^2+i0)[(Q-k)^2+i0](k^2-2k\cdot p+i0)(-v\cdot k+i0)}, \tag{18}$$

$$i\mathcal{M}_{\text{box}}^{(e)} = \frac{e^4}{2M} \int \frac{d^4k}{(2\pi)^4} \frac{[\bar{u}(p')\gamma^\mu(\not{p}-\not{k}+m_l)\gamma^\nu u(p)][\chi^\dagger(p'_p)\{v_\nu(p_p+p'_p+k)_\mu - v_\mu v_\nu(v\cdot k)\}\chi(p_p)]}{(k^2+i0)[(Q-k)^2+i0](k^2-2k\cdot p+i0)(v\cdot k+i0)}, \tag{19}$$

$$i\mathcal{M}_{\text{xbox}}^{(f)} = \frac{e^4}{2M} \int \frac{d^4k}{(2\pi)^4} \frac{[\bar{u}(p')\gamma^\mu(\not{p}-\not{k}+m_l)\gamma^\nu u(p)][\chi^\dagger(p'_p)\{v_\mu(2p'_p-k)_\nu - v_\mu v_\nu(-v\cdot k))\}\chi(p_p)]}{(k^2+i0)[(Q-k)^2+i0](k^2-2k\cdot p+i0)(-v\cdot k+i0)}, \tag{20}$$

$$i\mathcal{M}_{\text{box}}^{(g)} = \frac{e^4}{2M} \int \frac{d^4k}{(2\pi)^4} \frac{[\bar{u}(p')\gamma^\mu(\not{p}-\not{k}+m_l)\gamma^\nu u(p)][\chi^\dagger(p'_p)v_\mu v_\nu \chi(p_p)]}{(k^2+i0)[(Q-k)^2+i0](k^2-2k\cdot p+i0)} \left(1 + \frac{p_p^2}{(v\cdot k)^2} - \frac{(p_p+k)^2}{(v\cdot k)^2}\right), \tag{21}$$

$$i\mathcal{M}_{\text{xbox}}^{(h)} = \frac{e^4}{2M} \int \frac{d^4k}{(2\pi)^4} \frac{[\bar{u}(p')\gamma^\mu(\not{p}-\not{k}+m_l)\gamma^\nu u(p)][\chi^\dagger(p'_p)v_\mu v_\nu \chi(p_p)]}{(k^2+i0)[(Q-k)^2+i0](k^2-2k\cdot p+i0)} \left(1 + \frac{p_p'^2}{(v\cdot k)^2} - \frac{(p'_p-k)^2}{(v\cdot k)^2}\right), \tag{22}$$

$$i\mathcal{M}_{\text{seagull}}^{(i)} = \frac{2e^4}{2M} \int \frac{d^4k}{(2\pi)^4} \frac{[\bar{u}(p')\gamma^\mu(\not{p}-\not{k}+m_l)\gamma^\nu u(p)][\chi^\dagger(p'_p)(v_\mu v_\nu - g_{\mu\nu})\chi(p_p)]}{(k^2+i0)[(Q-k)^2+i0](k^2-2k\cdot p+i0)}, \tag{23}$$

where $u(p)$ and $\bar{u}(p')$ are the incoming and outgoing lepton Dirac spinors, and $\chi(p)$ and $\chi^\dagger(p'_p)$ are the proton's nonrelativistic two-component Pauli spinors. Here we remark that the two LO TPE integrals, Eqs. (15) and (16), should contain the kinetic energy terms of $\mathcal{O}(M^{-1})$ in the proton propagators [cf. Eq. (7)]. However, for the purpose of distinguishing the "true" LO from the NLO parts of the integrals, these $\mathcal{O}(M^{-1})$ terms from the two LO amplitudes have been included in the NLO propagator insertion integrals, Eqs. (21) and (22), respectively. In that case the first two amplitudes, namely, $\mathcal{M}_{\text{box}}^{(a)}$ and $\mathcal{M}_{\text{xbox}}^{(b)}$, correspond to the "true" LO contribution of the TPE.

All the rest contributing at NLO either correspond to terms that directly arise in the NLO chiral power counting or are attributed to the dynamical recoil $\mathcal{O}(M^{-1})$ terms moved from the LO chiral counting amplitudes. We isolate the IR divergences by taking the soft photon limit, which means: when one of the two photons' four-momenta is considered *soft* (either setting $k=0$ or $k=Q$) the other photon is *hard* [either with $(Q-k)^2 \neq 0$ or $k^2 \neq 0$]. To project out the IR singular terms, we must evaluate the loop integrals at both poles and then consider their sum.

To demonstrate the utility of this approach, let us apply SPA to the LO box, Eq. (15), and cross-box, Eq. (16),

amplitudes [cf. Figs. 1(a) and 1(b)]. Treating each of the two photons to be separately soft leads to the following sum of the amplitudes:

$$i\mathcal{M}_{\text{box}}^{(a)} \overset{\gamma_{\text{soft}}}{\rightsquigarrow} -2e^2(v\cdot p)\mathcal{M}_\gamma \int \frac{d^4k}{(2\pi)^4} \frac{1}{k^2(k^2-2k\cdot p)(v\cdot k+i0)}$$

$$-2e^2(v\cdot p')\mathcal{M}_\gamma \int \frac{d^4k}{(2\pi)^4} \frac{1}{k^2(k^2-2k\cdot p')(v\cdot k+i0)} \tag{24}$$

and

$$i\mathcal{M}_{\text{xbox}}^{(b)} \overset{\gamma_{\text{soft}}}{\rightsquigarrow} 2e^2(v\cdot p)\mathcal{M}_\gamma \int \frac{d^4k}{(2\pi)^4} \frac{1}{k^2(k^2-2k\cdot p)(v\cdot k-i0)}$$

$$+ 2e^2(v\cdot p')\mathcal{M}_\gamma \int \frac{d^4k}{(2\pi)^4}$$

$$\times \frac{1}{k^2(k^2-2k\cdot p')(v\cdot k-i0)}. \tag{25}$$

It is immediately clear that $\mathcal{M}_{\text{box}}^{(a)}$ is effectively canceled by $\mathcal{M}_{\text{xbox}}^{(b)}$, which apparently is not manifest otherwise.[6] Thus, we conclude that using the SPA the LO amplitudes of the TPE diagrams give no LO amplitude contributions in

HBχPT. This LO cancellation is anticipated since the proton does not generate any LO bremsstrahlung in HBχPT, *vis-à-vis* no LO IR divergence contributions in $\delta_{\text{IR}}^{(\text{soft})}$ [60]. A similar conclusion was obtained in Refs. [32,33], which evaluated the lepton-proton bremsstrahlung process ($\ell p \to \ell p\gamma$) using the same HBχPT framework.

The first nonvanishing TPE contributions in SPA arise from the NLO proton recoil contributions, which is commensurate with the corresponding nonzero HBχPT bremsstrahlung amplitudes with the soft photons radiated from NLO proton-photon vertices. We now analyze the NLO TPE integrals, Eqs. (17)–(23), and the following observations are in order:

(i) First, when we sum these amplitudes, the terms containing the $v_\mu v_\nu$ in the amplitudes $\mathcal{M}_{\text{box}}^{(c)}$ through $\mathcal{M}_{\text{box}}^{(f)}$ cancel with the first terms of amplitudes $\mathcal{M}_{\text{box}}^{(g)}$ and $\mathcal{M}_{\text{xbox}}^{(h)}$ plus the $v_\mu v_\nu$ part of the seagull term $\mathcal{M}_{\text{seagull}}^{(i)}$.

(ii) Second, applying SPA to the remaining parts of the two amplitudes, $\mathcal{M}_{\text{box}}^{(g)}$ and $\mathcal{M}_{\text{xbox}}^{(h)}$, we observe that they also cancel in the soft photon limits. This is easily seen by analyzing the remaining parts of the NLO proton propagator in each of these integrals in the following way:

$$i[\mathcal{M}_{\text{box}}^{(g)} + \mathcal{M}_{\text{xbox}}^{(h)}]_{\text{residual}} = \frac{e^4}{2M}\int \frac{d^4k}{(2\pi)^4}\cdots\left(\frac{p_p^2}{(v\cdot k)^2} - \frac{(p_p+k)^2}{(v\cdot k)^2} + \frac{p_p'^2}{(v\cdot k)^2} - \frac{(p_p'-k)^2}{(v\cdot k)^2}\right)$$

$$\overset{\gamma_{\text{soft}}}{\rightsquigarrow} \frac{e^4}{2M}\int \frac{d^4k}{(2\pi)^4}\cdots\left(\frac{\cancel{p_p^2}}{\cancel{(v\cdot k)^2}} - \frac{p_p^2}{\cancel{(v\cdot k)^2}} + \frac{\cancel{p_p'^2}}{(v\cdot k)^2} - \frac{\cancel{p_p'^2}}{(v\cdot k)^2}\right)_{k\to 0}$$

$$+ \frac{e^4}{2M}\int \frac{d^4k}{(2\pi)^4}\cdots\left(\frac{\cancel{p_p^2}}{\cancel{(v\cdot k)^2}} - \frac{\cancel{p_p'^2}}{(v\cdot k)^2} + \frac{\cancel{p_p'^2}}{(v\cdot k)^2} - \frac{\cancel{p_p^2}}{\cancel{(v\cdot k)^2}}\right)_{k\to Q} = 0. \tag{26}$$

Consequently, applying SPA, the two amplitudes, $\mathcal{M}_{\text{box}}^{(g)}$ and $\mathcal{M}_{\text{xbox}}^{(h)}$, which are the amplitudes with intermediate NLO proton propagator insertions, effectively do not contribute to the sum of the NLO TPE box amplitudes. Furthermore, we observe that in the seagull amplitude, Eq. (23), only the terms proportional to $g_{\mu\nu}$ contribute to the total TPE amplitude. The residual parts of the TPE integrals at NLO, after applying SPA to the box diagrams, yield the following simplified soft photon amplitudes[7]:

$$i\tilde{\mathcal{M}}_{\text{box}}^{(c)} = \frac{e^4}{M}(v\cdot p')\int \frac{d^4k}{(2\pi)^4}\frac{[\bar{u}(p')\gamma^\nu u(p)][\chi^\dagger(p'_p)(p_p+p'_p)_\nu\chi(p_p)]}{k^2Q^2(k^2-2k\cdot p')(v\cdot k+i0)}$$

$$- \frac{2e^2}{M}(p\cdot p_p)\mathcal{M}_\gamma \int \frac{d^4k}{(2\pi)^4}\frac{1}{k^2(k^2-2k\cdot p+i0)(v\cdot k+i0)}, \tag{27}$$

---

[6]Note the difference in the signs of the $\pm i\eta \to \pm i0$ terms in the heavy proton propagators of the two amplitudes contributes to a residual imaginary part, which is, however, irrelevant in the present context of evaluation of the unpolarized cross section.

[7]We do not apply SPA in the evaluation of the IR-finite seagull diagram. A *naive* application of SPA to this diagram leads to lepton self-energy-like contributions with spurious IR-divergent terms. However, an exact evaluation (see Appendix) shows no such singularities.

$$i\tilde{\mathcal{M}}_{\text{xbox}}^{(d)} = -\frac{e^4}{M}(v \cdot p)\int \frac{d^4k}{(2\pi)^4}\frac{[\bar{u}(p')\gamma^\mu u(p)][\chi^\dagger(p'_p)(p_p + p'_p)_\mu \chi(p_p)]}{k^2 Q^2(k^2 - 2k \cdot p)(v \cdot k - i0)}$$
$$+ \frac{2e^2}{M}(p' \cdot p_p)\mathcal{M}_\gamma \int \frac{d^4k}{(2\pi)^4}\frac{1}{k^2(k^2 - 2k \cdot p')(v \cdot k - i0)}, \tag{28}$$

$$i\tilde{\mathcal{M}}_{\text{box}}^{(e)} = \frac{e^4}{M}(v \cdot p)\int \frac{d^4k}{(2\pi)^4}\frac{[\bar{u}(p')\gamma^\mu u(p)][\chi^\dagger(p'_p)(p_p + p'_p)_\mu \chi(p_p)]}{k^2 Q^2(k^2 - 2k \cdot p)(v \cdot k + i0)}$$
$$- \frac{2e^2}{M}(p' \cdot p'_p)\mathcal{M}_\gamma \int \frac{d^4k}{(2\pi)^4}\frac{1}{k^2(k^2 - 2k \cdot p')(v \cdot k + i0)}, \tag{29}$$

$$i\tilde{\mathcal{M}}_{\text{xbox}}^{(f)} = -\frac{e^4}{M}(v \cdot p')\int \frac{d^4k}{(2\pi)^4}\frac{[\bar{u}(p')\gamma^\nu u(p)][\chi^\dagger(p'_p)(p_p + p'_p)_\nu \chi(p_p)]}{k^2 Q^2(k^2 - 2k \cdot p')(v \cdot k - i0)}$$
$$+ \frac{2e^2}{M}(p \cdot p'_p)\mathcal{M}_\gamma \int \frac{d^4k}{(2\pi)^4}\frac{1}{k^2(k^2 - 2k \cdot p)(v \cdot k - i0)}, \tag{30}$$

$$i\tilde{\mathcal{M}}_{\text{seagull}}^{(i)} = -\frac{e^4}{M}\int \frac{d^4k}{(2\pi)^4}\frac{[\bar{u}(p')\gamma^\mu(\not{p} - \not{k} + m_l)\gamma_\mu u(p)][\chi^\dagger(p'_p)\chi(p_p)]}{k^2(Q-k)^2(k^2 - 2k \cdot p + i0)}, \tag{31}$$

where the *tilde* symbols denote the residual NLO TPE amplitudes of Eqs. (17)–(23). Here we note again that there is a cancellation between $\tilde{\mathcal{M}}_{\text{box}}^{(c)}$ and $\tilde{\mathcal{M}}_{\text{xbox}}^{(f)}$ for the coefficient of $v \cdot p'$, and between $\tilde{\mathcal{M}}_{\text{xbox}}^{(d)}$ and $\tilde{\mathcal{M}}_{\text{box}}^{(e)}$ for the coefficient of $v \cdot p$ (up to an irrelevant imaginary part.) Then the resulting sum of the NLO TPE box amplitudes in the soft photon limit gets "factorized" into a Q^2 dependent function $f(Q^2)$ times the Born amplitude $\mathcal{M}_\gamma$ [56], namely,

$$\mathcal{M}_{\gamma\gamma}^{(\text{box})} \overset{\gamma_{\text{soft}}}{\rightsquigarrow} \tilde{\mathcal{M}}_{\gamma\gamma}^{(\text{box})} \equiv f(Q^2)\mathcal{M}_\gamma = \tilde{\mathcal{M}}_{\text{box}}^{(c)} + \tilde{\mathcal{M}}_{\text{xbox}}^{(d)} + \tilde{\mathcal{M}}_{\text{box}}^{(e)} + \tilde{\mathcal{M}}_{\text{xbox}}^{(f)}, \tag{32}$$

where

$$f(Q^2) = -\frac{2e^2}{M}[(p \cdot p_p)\mathcal{K}_v^{(+)}(p) - (p' \cdot p_p)\mathcal{K}_v^{(-)}(p') + (p' \cdot p'_p)\mathcal{K}_v^{(+)}(p') - (p \cdot p'_p)\mathcal{K}_v^{(-)}(p)]. \tag{33}$$

The integrals $\mathcal{K}_v^{(+)}$ and $\mathcal{K}_v^{(-)}$ are solved in D dimensions, i.e., $D > 4$ is the analytically continued spacetime dimension. In the expressions below, $\epsilon = (4 - D)/2$, μ corresponds to the subtraction scale, $\gamma_E = 0.577216\ldots$ is the Euler-Mascheroni constant, and the integrals $\mathcal{K}_v^{(\pm)}(p)$ in the above expression are given by

$$\mathcal{K}_v^{(+)}(p) = \frac{1}{i}\int \frac{d^4k}{(2\pi)^4}\frac{1}{k^2(k^2 - 2k \cdot p)(v \cdot k + i0)}$$
$$= -\frac{1}{(4\pi)^2 E\beta}\left[\left\{\frac{1}{\epsilon} - \gamma_E + \ln\left(\frac{4\pi\mu^2}{m_l^2}\right)\right\}\ln\sqrt{\frac{1+\beta}{1-\beta}} - \ln^2\sqrt{\frac{1+\beta}{1-\beta}} - \text{Sp}\left(\frac{2\beta}{1+\beta}\right) + \frac{\pi^2}{2}\right.$$
$$\left. - i\pi\left\{\frac{1}{\epsilon} - \gamma_E + \ln\left(\frac{\pi\mu^2}{E^2\beta^2}\right)\right\}\right],$$
$$\mathcal{K}_v^{(-)}(p) = \frac{1}{i}\int \frac{d^4k}{(2\pi)^4}\frac{1}{k^2(k^2 - 2k \cdot p)(v \cdot k - i0)}$$
$$= -\frac{1}{(4\pi)^2 E\beta}\left[\left\{\frac{1}{\epsilon} - \gamma_E + \ln\left(\frac{4\pi\mu^2}{m_l^2}\right)\right\}\ln\sqrt{\frac{1+\beta}{1-\beta}} - \ln^2\sqrt{\frac{1+\beta}{1-\beta}} - \text{Sp}\left(\frac{2\beta}{1+\beta}\right)\right], \tag{34}$$

where the term "Sp" stands for the standard *Spence function* defined as the integral

$$\mathrm{Sp}(z) = \int_0^z dt \frac{\ln(1-t)}{t}; \qquad z \in \mathbb{R}. \qquad (35)$$

Likewise, we find the expression for the integrals $\mathcal{K}_v^{(\pm)}(p')$ in Eq. (33) by replacing $E \leftrightarrow E'$ and $\beta \leftrightarrow \beta'$. The IR divergences correspond to the poles in the dimensionally regularized integrals in the limit $\epsilon = (4-D)/2 \to 0^-$. The appearance of an imaginary part in these integrals depends on the sign of the $\pm i\eta$ term as $\eta \to 0$ in the proton propagator. As mentioned, the imaginary parts are irrelevant in our present context of the unpolarized cross section analysis. Nevertheless, it might be interesting to note that an additional IR divergence arises in the imaginary part of $\mathcal{K}_v^{(+)}(p)$ which is of importance in a polarized cross section analysis.

Finally, we sum the TPE amplitudes and compute their interference with the Born amplitude in order to determine their contribution to the elastic cross section, with the appropriate IR singular term subtracted as shown in Eq. (10). To this end, the sum of the factorizable IR-divergent TPE box amplitudes with the nonfactorizable IR-free seagull amplitude (evaluated in Appendix) is given as

$$\mathcal{M}_{\gamma\gamma} = \tilde{\mathcal{M}}_{\gamma\gamma}^{(\mathrm{box})} + \tilde{\mathcal{M}}_{\mathrm{seagull}}^{(i)} = f(Q^2)\mathcal{M}_\gamma + \tilde{\mathcal{M}}_{\mathrm{seagull}}^{(i)}. \qquad (36)$$

Denoting the corresponding fractional TPE contributions to the elastic cross section as

$$\delta_{\gamma\gamma}(Q^2) = \delta_{\gamma\gamma}^{(\mathrm{box})}(Q^2) + \delta_{\gamma\gamma}^{(\mathrm{seagull})}(Q^2), \qquad (37)$$

we obtain the following NLO expressions,[8] noting that $E' = E + \mathcal{O}(M^{-1})$ and $\beta' = \beta + \mathcal{O}(M^{-1})$:

$$\delta_{\gamma\gamma}^{(\mathrm{box})}(Q^2) = \frac{2\mathcal{R}e\sum_{\mathrm{spins}}(\mathcal{M}_\gamma^* \tilde{\mathcal{M}}_{\gamma\gamma}^{(\mathrm{box})})}{\sum_{\mathrm{spins}}|\mathcal{M}_\gamma|^2} = 2\mathcal{R}e[f(Q^2)]$$

$$= -\frac{\alpha Q^2}{2\pi ME}\left[\left\{\frac{1}{\epsilon} - \gamma_E + \ln\left(\frac{4\pi\mu^2}{m_l^2}\right)\right\}\left\{\frac{1}{\beta}\ln\sqrt{\frac{1+\beta}{1-\beta}} + \frac{E}{E'\beta'}\ln\sqrt{\frac{1+\beta'}{1-\beta'}}\right\}\right.$$

$$\left. + \frac{1}{\beta}\left\{\frac{\pi^2}{2} - \ln^2\sqrt{\frac{1+\beta}{1-\beta}} - \mathrm{Sp}\left(\frac{2\beta}{1+\beta}\right)\right\} + \frac{E}{E'\beta'}\left\{\frac{\pi^2}{2} - \ln^2\sqrt{\frac{1+\beta'}{1-\beta'}} - \mathrm{Sp}\left(\frac{2\beta'}{1+\beta'}\right)\right\}\right]$$

$$= \delta_{\mathrm{IR}}^{(\mathrm{box})}(Q^2) - \frac{\alpha Q^2}{\pi ME\beta}\left[\frac{\pi^2}{2} + \ln\left(\frac{-Q^2}{m_l^2}\right)\ln\sqrt{\frac{1+\beta}{1-\beta}} - \ln^2\sqrt{\frac{1+\beta}{1-\beta}} - \mathrm{Sp}\left(\frac{2\beta}{1+\beta}\right)\right] + \mathcal{O}\left(\frac{1}{M^2}\right), \qquad (38)$$

for the TPE box contribution, with $\delta_{\mathrm{IR}}^{(\mathrm{box})}(Q^2) = -\delta_{\mathrm{IR}}^{(\mathrm{soft})}(Q^2)$ as given in Eq. (14), and the finite seagull contribution

$$\delta_{\gamma\gamma}^{(\mathrm{seagull})}(Q^2) = \frac{2\mathcal{R}e\sum_{\mathrm{spin}}(\mathcal{M}_\gamma^* \tilde{\mathcal{M}}_{\mathrm{seagull}}^{(i)})}{\sum_{\mathrm{spin}}|\mathcal{M}_\gamma|^2}$$

$$= -\frac{2\alpha Q^2}{\pi ME}\left[\frac{E^2 + EE'}{Q^2 + 4EE'}\right]\left(\mathcal{I}_1(Q^2) + \mathcal{I}_2(Q^2) + \frac{Q^2}{m_l^2}[\mathcal{I}_3(Q^2) - \mathcal{I}_4(Q^2)]\right)$$

$$= -\frac{4\alpha Q^2}{\pi ME}\left[\frac{E^2}{Q^2 + 4E^2}\right]\left(\mathcal{I}_1(Q^2) + \mathcal{I}_2(Q^2) + \frac{Q^2}{m_l^2}[\mathcal{I}_3(Q^2) - \mathcal{I}_4(Q^2)]\right) + \mathcal{O}\left(\frac{1}{M^2}\right). \qquad (39)$$

The integrals $\mathcal{I}_i$ ($i = 1$–4) are presented in Appendix where we evaluate the seagull term. We subsequently use Eq. (10) to obtain the finite TPE contribution in SPA. As mentioned, $\delta_{\mathrm{IR}}^{(\mathrm{box})}$ cancels exactly with $\delta_{\mathrm{IR}}^{(\mathrm{soft})}$ when we include the soft bremsstrahlung contribution to this order in QED.

IV. RESULTS AND DISCUSSION

Next we present numerical estimates of the analytically derived expressions for the box and seagull TPE contributions obtained in the previous section. Figure 3 displays our results showing the dependence of the finite fractional TPE corrections, $\bar{\delta}_{\gamma\gamma}$, of the ep and μp elastic

---

[8]Since the corrections in Eqs. (38) and (39) originate at NLO, we use the LO expression for the four-momentum transferred, i.e., $Q^2 \to Q_0^2 = -2\beta^2 E^2(1 - \cos\theta)$.
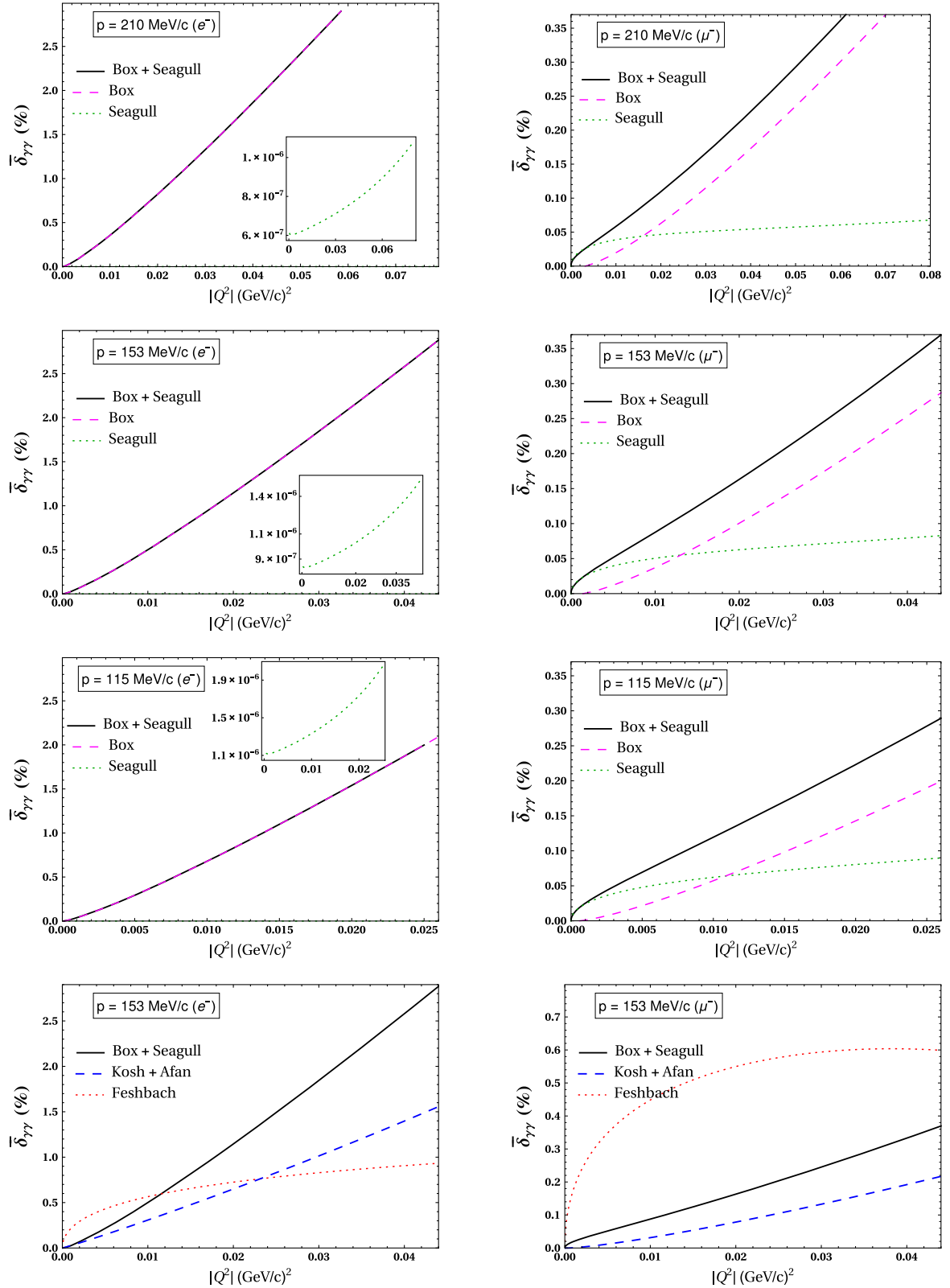
FIG. 3.   Comparison of the finite TPE contributions for the box and seagull diagrams to the ep (left panel) and μp (right panel) elastic scattering cross sections as a function of the squared four-momentum transfer $|Q^2|$ given at the three proposed MUSE incoming lepton momenta, namely, 210 MeV/c, 153 MeV/c, and 115 MeV/c. The seagull contributions for the ep scattering, being numerically much smaller, are shown within the inset plots. The plots in the bottom panel (fourth row) show the comparison of our results (for incoming lepton momentum, $p = 153$ MeV/c) with the qualitatively similar TPE results from the recent relativistic hadronic model calculation of Ref. [57] (labeled as "Kosh + Afan"). The contribution of the Feshbach term of Ref. [34] (labeled as "Feshbach") is also displayed.

scattering versus the squared four-momentum transfer at $\mathcal{O}(\alpha, M^{-1})$. The results displayed in the figure indicate that the TPE corrections for electron-proton scattering goes up to about 4.5% and that for the muon-proton scattering up to around 0.5% for the largest MUSE incoming momentum. As anticipated from recent TPE works, e.g., Refs. [19,30,57], our TPE contributions are vanishing when Q^2 becomes zero.[9] As observed in the figure, the TPE contributions for electron-proton scattering are about an order of magnitude larger than for muon-proton scattering. At a given $|Q^2|$ and for increasing incident MUSE lepton momenta, $\bar{\delta}_{\gamma\gamma}$ becomes smaller but the relative electron-proton to muon-proton ratio for $\bar{\delta}_{\gamma\gamma}$ stays almost the same. In Fig. 3 we also compare our evaluations of the TPE box, $\bar{\delta}_{\gamma\gamma}^{(\text{box})}$, and the seagull, $\delta_{\gamma\gamma}^{(\text{seagull})}$, contributions. Here we note that in relativistic QED the TPE box (and cross-box) diagrams give the TPE amplitude, whereas in HBχPT the baryons being treated nonrelativistically, the seagull diagram naturally appears. In this case, the magnitude of the finite seagull contribution is found to be quite insensitive to the Q^2 dependence except when $Q^2 \to 0$. For

electron-proton scattering, the seagull contribution is more or less inconsequential yielding a minuscule contribution, i.e., $\sim 10^{-6}$% for the range of MUSE kinematics, while for the muon-proton scattering its contribution is much larger going up to about 0.06%. The TPE box diagrams, however, mostly dominate the entire MUSE range of momentum transfers. An exception only occurs for muon-proton scattering in the region, $Q^2 \lesssim 0.01$ $(\text{GeV}/c)^2$, where our result indicates that the seagull terms become numerically larger than the box contributions.

The TPE results of Ref. [57], which we label as "Kosh + Afan," are compared with our evaluations in the bottom panels of Fig. 3, when we adjust their expressions to reflect our IR treatment of the TPE amplitude. To be specific, in the method used for comparing the TPE results, we consider only the relevant finite part of their TPE result [cf. Eq. (20) in Ref. [57]], leaving out the IR singular terms which must cancel against those from soft bremsstrahlung. In our notation Eq. (20) of Ref. [57] for the TPE (adjusted by a constant factor such that it vanishes at $Q^2 = 0$) in the SPA is written as follows:

$$\bar{\delta}_{\gamma\gamma}(Q^2)|_{\text{Ref [57]}} = -\frac{\alpha}{\pi}\left[-\frac{b_{11}}{\gamma_{11}}\left\{ \ln\left(\frac{-Q^2}{m_l M}\right) + \frac{1}{2}\ln\alpha_{12} \cdot \ln\left(\frac{4\gamma_{11}^2}{m_l^4 \alpha_{11}(1-\alpha_{11})^2}\right) \right.\right.$$
$$\left. + \text{Sp}\left(\frac{\alpha_{11}(m_l^2 - b_{11} + M^2)}{2\gamma_{11}(1-\alpha_{11})}\right) - \text{Sp}\left(\frac{m_l^2 - b_{11} + M^2}{2\gamma_{11}(1-\alpha_{11})}\right) \right\}$$
$$+ \frac{b_{12}}{\gamma_{12}}\left\{ \ln\left(\frac{-Q^2}{m_l M}\right) + \frac{1}{2}\ln\alpha_{12} \cdot \ln\left(\frac{4\gamma_{12}^2}{m_l^4 \alpha_{12}(1-\alpha_{12})^2}\right) \right.$$
$$\left.\left. + \text{Sp}\left(\frac{\alpha_{12}(m_l^2 - b_{12} + M^2)}{2\gamma_{12}(1-\alpha_{12})}\right) - \text{Sp}\left(\frac{m_l^2 - b_{12} + M^2}{2\gamma_{12}(1-\alpha_{12})}\right) \right\}\right], \tag{40}$$

where

$$b_{11} = 2EM, \qquad b_{12} = Q^2 + b_{11},$$
$$\alpha_{11} = \frac{b_{11} + 2\gamma_{11}}{2m_l^2}, \qquad \gamma_{11} = \frac{1}{2}\sqrt{b_{11}^2 - 4m_l^2 M^2},$$
$$\alpha_{12} = \frac{b_{12} + 2\gamma_{12}}{2m_l^2}, \qquad \gamma_{12} = \frac{1}{2}\sqrt{b_{12}^2 - 4m_l^2 M^2}. \tag{41}$$

In order to facilitate the comparison with our dimensionally regularized TPE expression $\bar{\delta}_{\gamma\gamma}(Q^2)$ [cf. Eqs. (10), (38), and (39)] we modify their analytically regularized IR

singular terms proportional to $\ln\lambda^2$, where λ is a fictitious photon mass, in the following way:

$$\ln\left(\frac{\lambda^2}{m_l M}\right) \mapsto \ln\left(\frac{-Q^2}{m_l M}\right) + \ln\left(\frac{\lambda^2}{-Q^2}\right). \tag{42}$$

Note that the IR-divergent terms proportional to $\ln\lambda^2$ for the TPE correction gets canceled by similar IR terms from a soft photon bremsstrahlung process leading to their finite expression, Eq. (38) in Ref. [57]. We observe in Fig. 3 that the overall low-$|Q^2|$ behavior of our TPE contributions is roughly consistent with Ref. [57] SPA results which are based on the use of relativistic pointlike (Dirac) protons. Nevertheless, despite the apparent qualitative similarity, our total TPE contribution differs in magnitude roughly by about a factor of 2 from that in Ref. [57]. Moreover, we note that our results substantially differ from the results of another recent TPE work, Ref. [30], which evaluated the box diagrams for muon-proton scattering using a

---

[9]It may be noted that in Ref. [57] a direct evaluation of the TPE [cf. Eq. (20) of this reference] leads to a nonzero contribution at $Q^2 = 0$, and hence, needed to be shifted by a constant factor to provide physical justification of vanishing asymmetry at $Q^2 = 0$. However, we checked that an expansion of their Eq. (20) to $\mathcal{O}(1/M)$ indeed vanishes at $Q^2 = 0$.

relativistic hadronic model. However, unlike Ref. [57] and our work, the authors of Ref. [30] did not employ SPA in their calculations, and instead numerically evaluated the TPE amplitudes involving the so-called *four-point integrals* [63,64] and their derivatives. In addition, they isolated the IR singular terms analytically from their TPE amplitude according to the Maximon and Tjon prescription [23]. The significant difference of our TPE correction as well as the results of Ref. [57] from those in Ref. [30] may imply that a part of the TPE box diagram loop integration involves contributions from two "hard" photon exchanges in muon-proton scattering. This is precisely the integration region of these TPE loops excluded in SPA.

Furthermore, in Fig. 3 we compare our TPE results with the Coulomb potential scattering result in the second Born approximation by McKinley and Feshbach [34], labeled "Feshbach" in the figure. As shown in Refs. [30,47], the relativistic evaluation of the TPE diagrams for a pointlike Dirac proton without SPA are qualitatively very similar to the Feshbach contribution for muon-proton scattering. Nevertheless, it may be worth noting that the original Feshbach derivation is applicable only for ultrarelativistic electrons. As seen in Fig. 3 for the electron-proton scattering, our results as well as those in Ref. [57] are comparable to the Feshbach term for low-$|Q^2|$ values, thereby indicating that the "hard" photon TPE loop contributions might not be too important for electron-proton scattering.

It is also instructive to study the TPE dependence on the virtual photon "polarization" flux factor ε which may be expressed in terms of the four-momentum transfer Q^2 by the relation [30]

$$\varepsilon(Q^2) = \frac{16\nu^2 + Q^2(4M^2 - Q^2)}{16\nu^2 - (4M^2 - Q^2)(4m_l^2 + Q^2)}, \quad (43)$$

where $\nu = (s - u)/4 = (4EM + Q^2)/4$ is the crossing symmetric variable in the target rest frame. For fixed incident lepton beam momenta, the full kinematically allowed elastic scattering range, namely, $0 < \theta < \pi$ and $0 < |Q^2| < |Q^2_{\text{max}}|$ [cf. below Eq. (8)], yields the physical bound on the flux factor, namely, $\varepsilon_{\text{max}} > \varepsilon > \varepsilon_{\text{min}}$, where

$$\varepsilon_{\text{max}} \equiv \varepsilon(0) = \frac{1}{\beta^2},$$

$$\varepsilon_{\text{min}} \equiv \varepsilon(Q^2_{\text{max}}) = \frac{m_l^2(m_l^2 + M^2 + 2EM)}{2\beta^2 E^2 M^2}. \quad (44)$$

While for fixed four-momentum transfers, if $|Q^2| > 2m_l^2$, then $2m_l^2/|Q^2| < \varepsilon < 1$, and if $|Q^2| < 2m_l^2$, then $1 < \varepsilon < 2m_l^2/|Q^2|$. The critical case, $|Q^2| = |Q^2_{\text{crit}}| = 2m_l^2$, corresponds to $\varepsilon = 1$ for all possible incoming lepton momenta. It is worth noting that for the massless lepton case, ε may be interpreted as the longitudinal polarization of the photon in
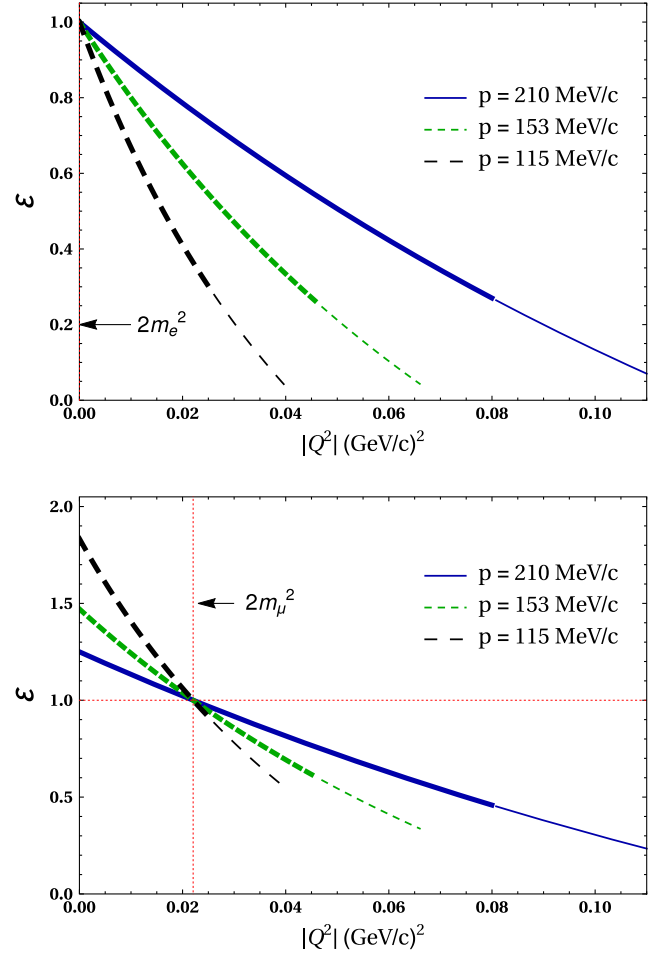

FIG. 4. The dependence of the virtual photon "polarization" factor ε on the squared four-momentum transfer $|Q^2|$ for the proposed MUSE beam momenta for ep scattering (upper panel) and μp scattering (lower panel.) Each plot corresponds to the full kinematically allowed scattering range $0 < |Q^2| < |Q^2_{\text{max}}|$ when $\theta \in [0, \pi]$ (thin lines). The thick lines are associated with the MUSE kinematic range where $\theta \in [20°, 100°]$. The curves intersect at $\varepsilon = 1$, which correspond to the critical values, $|Q^2_{\text{crit}}| = 2m_e^2 = 5 \times 10^{-7}$ $(\text{GeV}/c)^2$ and $|Q^2_{\text{crit}}| = 2m_\mu^2 = 0.02205$ $(\text{GeV}/c)^2$.

the case of one-photon exchange [30]. Figure 4 displays the $|Q^2|$ dependence of ε for ep and μp elastic scatterings. The figure identifies both the kinematically allowed and the relevant MUSE range of ε values. Correspondingly, Fig. 5 displays the ε dependence of our TPE corrections for three specific choices of $|Q^2|$, namely, 0.005 $(\text{GeV}/c)^2$, 0.01 $(\text{GeV}/c)^2$, and 0.02 $(\text{GeV}/c)^2$. In each case of fixed $|Q^2|$ the TPE effects vanish as $\varepsilon \to 1$, i.e., the forward scattering limit, and tend toward maximum as $\varepsilon \to 2m_l^2/|Q^2|$ for backward scatterings [19], as reflected in Fig. 5. This feature of our TPE result is again qualitatively similar to the result obtained in Ref. [57] but contrasts sharply with the Feshbach result [34] as well as that of Ref. [30].
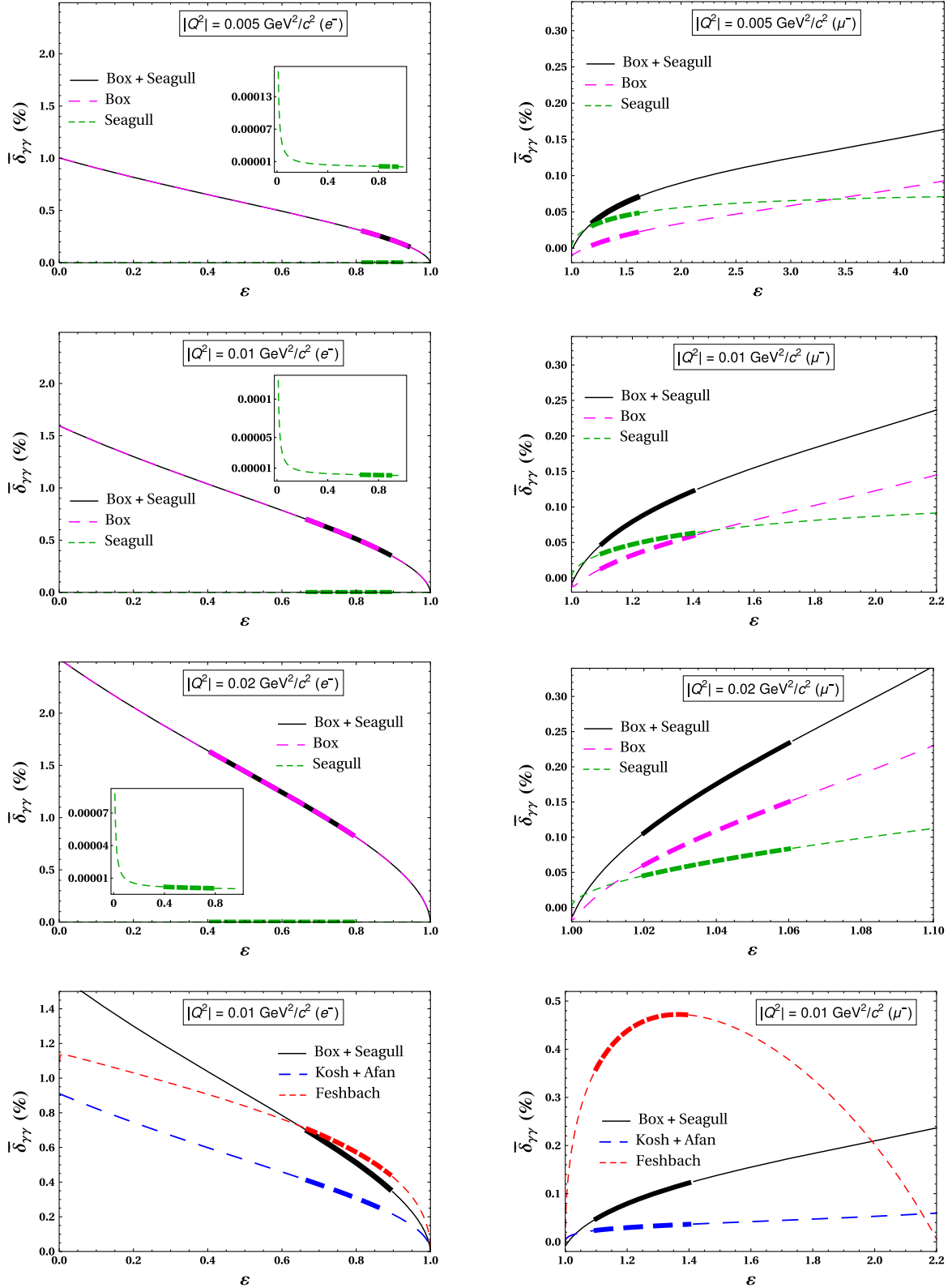
FIG. 5. The ε dependence of the finite TPE contributions for ep (left panel) and μp (right panel) elastic cross sections for three specific $|Q^2|$ values in the proposed MUSE kinematic range. The seagull contributions for the ep scattering being numerically much smaller are shown within the inset plots. The plots in the bottom panel (fourth row) show the comparison of our results for $|Q^2| = 0.01$ $(\text{GeV}/c)^2$ with the qualitatively similar results from Ref. [57] (labeled as "Kosh + Afan"). The contribution of the Feshbach term [34] (labeled as "Feshbach") is also displayed. Each plot corresponds to the kinematically allowed range of ε when $\theta \in [0, \pi]$ (thin lines), and the "segment" relevant to the MUSE kinematic range with $\theta \in [20°, 100°]$ (thick lines).

V. SUMMARY AND CONCLUSION

We present a low-energy model-independent calculation of the two-photon exchange contributions to the lepton-proton elastic unpolarized cross section at next-to-leading order in HBχPT. The lepton mass is included in all our expressions. Our approach contrasts many previous TPE evaluations using relativistic hadronic models which often use phenomenological form factors to parametrize the proton-photon vertices. In HBχPT the heavy proton is treated in a manifestly nonrelativistic framework which makes it ideal for investigating the structure of the proton at very low momentum transfers. Our evaluation is based on the assumption that the most dominant contributions to the TPE loop diagrams arise from the elastic proton inter-mediate state while inelastic contributions are considered small for low-$|Q^2|$ values. This is especially relevant in the proposed low-energy MUSE kinematic domain where incoming lepton beam momenta are between $p = 115$ and 210 MeV/c. We note that while most other works use analytic regularization schemes with a nonzero photon mass, we used the gauge invariant prescription of the dimensional regularization scheme to isolate the infrared singularities of the two-photon loops. In this approach, however, the exact evaluation of the IR-divergent four-point one-loop Green's function [63,64] demands analytical evaluations of D-dimensional integrals which to the best of our knowledge have not been pursued for exchanges of massless photons. Further, we demonstrated in Sec. III that the soft photon limit was taken only after the cancellations among the NLO amplitudes were taken into account. Moreover, one should bear in mind that we restricted the soft photon approximation only to the IR-divergent diagrams. Thus, we evaluated the IR-free seagull diagram without invoking the soft photon approximation.

The evaluation of the TPE box diagrams (with exchange bosons with nonzero masses) involves scalar and tensor four-point loop integrals, a topic that has been discussed extensively in many previous works, e.g., Refs. [63–67]. In the pioneering works of Refs. [63,64], such tensor integrals were reduced to scalar one-loop *master* integrals involving one-, two-, three-, and four-point functions which were evaluated analytically using the dimensional regularization scheme. The work of Ref. [67] extended the above formalism to include heavy-fermion propagators. However, these approaches are unsuitable for dealing with IR divergences using dimensional regularization with massless photon exchanges. In fact, for massless photon exchanges the exact analytical evaluation of the IR-divergent four-point functions in dimensional regularization remains an open issue. Nevertheless, using dimensional regularization with the soft photon approximation provides a viable alternative for the reduction of the four-point scalar integrals into well-known standard ones. This approximation allows us to easily project out the IR-divergent parts of the TPE box diagrams in order to

obtain a finite contribution to the elastic cross section. In the soft photon limit the four-point loop integral reduces to a three-point integrals which can be evaluated analyti-cally, wherein each of the TPE loop momentum, $0 \leq (k_0, |\mathbf{k}|) \leq \infty$, can be decomposed as a sum of two integrals each with a hard and a soft photon. The contributions from two simultaneous hard photon exchanges are ignored in the soft photon limit.

The results for the electron-proton scattering seem to indicate that the dominant contribution from the TPE loop momenta are expected to arise from the integration domain where the contribution of the two hard photon exchanges may give small contributions. In contrast, it appears that for muon-proton scattering the hard two-photon exchange part of the TPE loops could give significant contributions. This conclusion is based on a comparison with the muon-proton scattering analysis presented in Ref. [47] (cf. Fig. 2 of this reference), where the TPE amplitude was evaluated relativistically with pointlike protons. This may indicate the importance of including two hard photon exchanges even in very low-energy muon-proton scattering for a more robust estimation of the TPE contribution.

In conclusion, we demonstrated in this paper many cancellations among the NLO box and seagull diagrams, which are likely to remain approximately valid beyond SPA. Furthermore, we showed that while the LO TPE contributions vanish (up to an irrelevant imaginary part), the dominant TPE effects arise from the box diagrams with NLO proton-photon vertices except at very low-$|Q^2|$ values where the finite seagull terms become significantly large for muon-proton scattering. However, the seagull diagram gives only a tiny contribution for electron-proton scattering at MUSE energies. We find that the low-$|Q^2|$ behavior of our TPE contributions are in rough agreement with the results in Ref. [57], although they differ substantially from those in Ref. [30]. As a next step it could be desirable to use standard numerical packages in order to evaluate the TPE box diagrams in the heavy baryon scheme and to examine the robustness of our soft photon approximation results. An estimate of the NNLO corrections in HBχPT that include, e.g., the contribution of pion loops and the proton's magnetic moment, would also be helpful in understanding the uncertainties using the HBχPT approach. Additionally, the inelastic Δ intermediate TPE contributions may be included to constrain uncertainties.

APPENDIX: DETAILED DERIVATION OF THE SEAGULL AMPLITUDE

Here we derive the TPE seagull amplitude $\mathcal{M}^{(i)}_{\text{seagull}}$ from diagram (i) in Fig. 1. The integral in Eq. (23) being both IR and UV finite does not require any regularization and is evaluated analytically in the four-dimensional spacetime. In Sec. III, it was shown *without* implementing SPA that due to cancellations among various NLO TPE amplitudes only the residual part of $\tilde{\mathcal{M}}^{(i)}_{\text{seagull}}$ proportional to $g^{\mu\nu}$ contributes to the cross section, namely,

$$
\begin{aligned}
\tilde{\mathcal{M}}^{(i)}_{\text{seagull}} &= -\frac{e^4}{M}\frac{1}{i}\int\frac{d^4k}{(2\pi)^4} \\
&\quad \times \frac{[\bar{u}(p')\gamma^\mu(\not{p}-\not{k}+m_l)\gamma_\mu u(p)][\chi^\dagger(p'_p)\chi(p_p)]}{k^2(Q-k)^2(k^2-2k\cdot p+i0)} \\
&= -\frac{e^4}{M}[\bar{u}(p')\gamma^\alpha \mathbb{I}_{\text{seagull}}\gamma_\alpha u(p)][\chi^\dagger(p'_p)\chi(p_p)],
\end{aligned}
$$

(A1)

where the loop-integral appearing above is given by

$$
\mathbb{I}_{\text{seagull}} = \frac{1}{i}\int\frac{d^4k}{(2\pi)^4}\frac{\not{p}-\not{k}+m_l}{(k^2+i0)(Q-k)^2(k^2-2k\cdot p+i0)},
$$

where k and $Q-k$ are the momenta of the two exchanged photons and $Q=p-p'$. Using Feynman parametrization and thereby shifting the integration variable, $k\to k+\beta$ where $\beta=(px+Qy)$ yields

$$
\begin{aligned}
\mathbb{I}_{\text{seagull}} &= \frac{1}{i}\int_0^1\int_0^1\int_0^1 dx\,dy\,dz\,\delta(1-x-y-z) \\
&\quad \times \int\frac{d^4k}{(2\pi)^4}\frac{2(\not{p}-\not{k}-\not{\beta}+m_l)}{[k^2-\Delta]^3}.
\end{aligned}
$$

Integration over the loop momentum k, we obtain

$$
\begin{aligned}
\mathbb{I}_{\text{seagull}} &= -\frac{1}{16\pi^2}\int_0^1\int_0^1\int_0^1 dx\,dy\,dz\,\delta(1-x-y-z) \\
&\quad \times \left[\frac{\not{p}-\not{\beta}+m_l}{\Delta}\right],
\end{aligned}
$$

(A2)

where $\Delta=(px+Qy)^2-Q^2y$. Further, it is convenient to make a change of variables from (x,y,z) to (ω,ξ) using the transformation $x=\omega\xi$, $y=\omega(1-\xi)$, and $z=1-\omega$, which amounts to the following change of the integration measures, namely, $dx\,dy\,dz\,\delta(1-x-y-z)\mapsto\omega\,d\omega\,d\xi$. Thus, we obtain

$$
\begin{aligned}
\mathbb{I}_{\text{seagull}} &= -\frac{1}{16\pi^2}\int_0^1\int_0^1 d\omega\,d\xi\frac{m_l+\not{p}(1-\omega\xi)-\not{Q}\omega(1-\xi)}{[\omega(m_l^2\xi^2-Q^2\xi+Q^2)-Q^2(1-\xi)]} \\
&= -\frac{1}{16\pi^2}\int_0^1\int_0^1 d\omega\,d\xi\left[\frac{m_l+\not{p}}{\omega(m_l^2\xi^2-Q^2\xi+Q^2)+Q^2(\xi-1)}-\frac{\omega[\not{Q}+\xi(\not{p}-\not{Q})]}{\omega(m_l^2\xi^2-Q^2\xi+Q^2)+Q^2(\xi-1)}\right] \\
&= -\frac{1}{16\pi^2 m_l^2}\left[(m_l+\not{p})\mathcal{I}_1-(\not{p}-\not{Q})\left(\mathcal{I}_2+\frac{Q^2}{m_l^2}\mathcal{I}_3\right)-(2\not{Q}-\not{p})\frac{Q^2}{m_l^2}\mathcal{I}_4+\not{Q}\left(\frac{Q^2}{m_l^2}\mathcal{I}_5-\mathcal{I}_6\right)\right]
\end{aligned}
$$

(A3)

with

$$
\mathcal{I}_1(Q^2)=\int_0^1 d\xi\left[\frac{1}{\xi^2-\frac{Q^2}{m_l^2}\xi+\frac{Q^2}{m_l^2}}\right]\ln\left[\frac{m_l^2\xi^2}{Q^2(\xi-1)}\right], \qquad \mathcal{I}_2(Q^2)=\int_0^1 d\xi\left[\frac{\xi}{\xi^2-\frac{Q^2}{m_l^2}\xi+\frac{Q^2}{m_l^2}}\right],
$$

$$
\mathcal{I}_3(Q^2)=\int_0^1 d\xi\left[\frac{\xi}{\xi^2-\frac{Q^2}{m_l^2}\xi+\frac{Q^2}{m_l^2}}\right]^2\ln\left[\frac{m_l^2\xi^2}{Q^2(\xi-1)}\right], \qquad \mathcal{I}_4(Q^2)=\int_0^1 d\xi\left[\frac{\xi}{(\xi^2-\frac{Q^2}{m_l^2}\xi+\frac{Q^2}{m_l^2})^2}\right]\ln\left[\frac{m_l^2\xi^2}{Q^2(\xi-1)}\right],
$$

$$
\mathcal{I}_5(Q^2)=\int_0^1 d\xi\left[\frac{1}{\xi^2-\frac{Q^2}{m_l^2}\xi+\frac{Q^2}{m_l^2}}\right]^2\ln\left[\frac{m_l^2\xi^2}{Q^2(\xi-1)}\right], \qquad \mathcal{I}_6(Q^2)=\int_0^1 d\xi\left[\frac{1}{\xi^2-\frac{Q^2}{m_l^2}\xi+\frac{Q^2}{m_l^2}}\right].
$$

(A4)

Each of the above integrals are easily obtainable in closed forms using standard techniques or with *Mathematica*. Since some of these integrals have rather elaborate expressions, we prefer to omit their explicit expressions in this communication. Inserting the loop amplitude $\mathbb{I}_{\text{seagull}}$ into Eq. (A1) we obtain our final expression for the seagull amplitude,

$$
\tilde{\mathcal{M}}^{(i)}_{\text{seagull}} = \frac{\alpha^2}{m_l^2 M}\left[\mathcal{N}_1\mathcal{I}_1-\mathcal{N}_2\left(\mathcal{I}_2+\frac{Q^2}{m_l^2}\mathcal{I}_3\right)-\mathcal{N}_3\left(\mathcal{I}_6-\frac{Q^2}{m_l^2}\mathcal{I}_5\right)-\mathcal{N}_4\frac{Q^2}{m_l^2}\mathcal{I}_4\right],
$$

(A5)

where $\mathcal{N}_i\propto\mathcal{M}_\gamma$ $(i=1,\ldots,4)$ are defined as

$$\mathcal{N}_1 = [\bar{u}(p')\gamma^\mu(m_l + \not{p})\gamma_\mu u(p)][\chi_p^\dagger(p'_p)\chi_p(p_p)],$$

$$\mathcal{N}_2 = [\bar{u}(p')\gamma^\mu(\not{p} - \mathcal{Q})\gamma_\mu u(p)][\chi_p^\dagger(p'_p)\chi_p(p_p)],$$

$$\mathcal{N}_3 = [\bar{u}(p')\gamma^\mu \mathcal{Q}\gamma_\mu u(p)][\chi_p^\dagger(p'_p)\chi_p(p_p)],$$

$$\mathcal{N}_4 = [\bar{u}(p')\gamma^\mu(2\mathcal{Q} - \not{p})\gamma_\mu u(p)][\chi_p^\dagger(p'_p)\chi_p(p_p)]. \quad \text{(A6)}$$

Thus, in essence we find that the seagull amplitude, unlike the TPE box amplitudes in SPA, *does not* naturally factorize into the LO amplitude $\mathcal{M}_\gamma$ times a Q^2 dependent function $f(Q^2)$. This result is consistent with the proposition made in Ref. [56] that the one-loop virtual radiative corrections, and in particular the TPE amplitudes, can be expressed as, $\mathcal{M}_{1-\text{Loop}} = f(Q^2)\mathcal{M}_\gamma + \bar{\mathcal{M}}_{1-\text{Loop}}$. The factorizable IR-divergent first term constitutes the dominant, so-called *outer corrections*, independent of the hadron structure, while the nonfactorizable IR-finite second term constitutes small corrections, the so-called *inner corrections*. In most works these latter corrections are hadron structure dependent and are often ignored in ultrarelativistic approximations. In the HBχPT approach we find that the dominant TPE box diagrams in SPA can be identified with the former corrections, while the seagull term can be identified with the latter ones. At the order of our accuracy, the latter corrections are free of low-energy constants and, therefore, are hadron structure independent.

Finally, it is noteworthy that, while determining $\delta_{\gamma\gamma}^{(\text{seagull})}$, Eq. (39), the integrals $\mathcal{I}_5$ and $\mathcal{I}_6$ drop out of the calculation due to the vanishing of spin trace of $\mathcal{N}_3$ with $\mathcal{M}_\gamma$, Eq. (11). We find

$$\sum_{\text{spins}} \mathcal{M}_\gamma^* \mathcal{N}_3 = 0 \quad \text{(A7)}$$

and

$$\sum_{\text{spins}} \mathcal{M}_\gamma^* \mathcal{N}_1 = -\sum_{\text{spins}} \mathcal{M}_\gamma^* \mathcal{N}_2 = \sum_{\text{spins}} \mathcal{M}_\gamma^* \mathcal{N}_4$$

$$= -\frac{16e^2 m_l^2}{Q^2}(E + E')(E_p + M)(E'_p + M)$$

$$= -\frac{128e^2 m_l^2 M^2 E}{Q^2}\left[1 + \mathcal{O}\left(\frac{1}{M}\right)\right]. \quad \text{(A8)}$$

Here we have used $E' = E + \mathcal{O}(M^{-1})$ and $E'_p = M + \mathcal{O}(M^{-1})$, since the seagull diagram already is an NLO amplitude.

[1] R. Pohl *et al.*, Nature (London) **466**, 213 (2010).
[2] A. Antognini *et al.*, Science **339**, 417 (2013).
[3] P. J. Mohr, D. B. Newell, and B. N. Taylor (Codata Collaboration), Rev. Mod. Phys. **88**, 035009 (2016).
[4] R. Pohl, R. Gilman, G. A. Miller, and K. Pachucki, Annu. Rev. Nucl. Part. Sci. **63**, 175 (2013).
[5] J. Bernauer *et al.* (A1 Collaboration), Phys. Rev. Lett. **105**, 242001 (2010).
[6] X. Zhan *et al.*, Phys. Lett. B **705**, 59 (2011).
[7] M. Mihovilovič *et al.*, Phys. Lett. B **771**, 194 (2017).
[8] N. Bezginov, T. Valdez, M. Horbatsch, A. Marsman, A. C. Vutha, and E. A. Hessels, Science **365**, 1007 (2019).
[9] R. C. Walker *et al.*, Phys. Rev. D **49**, 5671 (1994).
[10] P. E. Bosted, Phys. Rev. C **51**, 409 (1995).
[11] B. D. Milbrath *et al.*, Phys. Rev. Lett. **80**, 452 (1998).
[12] B. D. Milbrath *et al.*, Phys. Rev. Lett. **82**, 2221(E) (1999).
[13] M. K. Jones *et al.*, Phys. Rev. Lett. **84**, 1398 (2000).
[14] O. Gayou *et al.*, Phys. Rev. C **64**, 038202 (2001).
[15] O. Gayou *et al.*, Phys. Rev. Lett. **88**, 092301 (2002).
[16] E. J. Brash, A. Kozlov, S. Li, and G. M. Huber, Phys. Rev. C **65**, 051001 (2002).
[17] J. Arrington, Phys. Rev. C **68**, 034325 (2003).
[18] C. F. Perdrisat, V. Punjabi, and M. Vanderhaeghen, Prog. Part. Nucl. Phys. **59**, 694 (2007).
[19] J. Arrington, P. G. Blunden, and W. Melnitchouk, Prog. Part. Nucl. Phys. **66**, 782 (2011).
[20] C. E. Carlson, Prog. Part. Nucl. Phys. **82**, 59 (2015).
[21] Y.-S. Tsai, Phys. Rev. **122**, 1898 (1961).

[22] L. W. Mo and Y.-S. Tsai, Rev. Mod. Phys. **41**, 205 (1969).
[23] L. C. Maximon and J. A. Tjon, Phys. Rev. C **62**, 054320 (2000); Rev. Mod. Phys. **41**, 193 (1969).
[24] M. Vanderhaeghen, J. M. Friedrich, D. Lhuillier, D. Marchand, L. Van Hoorebeke, and J. Van de Wiele, Phys. Rev. C **62**, 025501 (2000).
[25] A. V. Gramolin, V. S. Fadin, A. L. Feldman, R. E. Gerasimov, D. M. Nikolenko, I. A. Rachek, and D. K. Toporkov, J. Phys. G **41**, 115001 (2014).
[26] A. Gasparian (PRad Collaboration), EPJ Web Conf. **73**, 07006 (2014).
[27] C. Peng and H. Gao (PRad Collaboration), EPJ Web Conf. **113**, 03007 (2016).
[28] R. Gilman *et al.* (MUSE Collaboration), arXiv:1303.2160.
[29] R. Gilman, AIP Conf. Proc. **1563**, 167 (2013).
[30] O. Tomalak and M. Vanderhaeghen, Phys. Rev. D **90**, 013006 (2014).
[31] A. Afanasev, P. G. Blunden, D. Hasell, and B. A. Raue, Prog. Part. Nucl. Phys. **95**, 245 (2017).
[32] P. Talukdar, F. Myhrer, G. Meher, and U. Raha, Eur. Phys. J. A **54**, 195 (2018).
[33] F. Myhrer, P. Talukdar, and U. Raha, Few Body Syst. **59**, 62 (2018).
[34] W. A. McKinley and H. Feshbach, Phys. Rev. **74**, 1759 (1948).
[35] C. E. Carlson and M. Vanderhaeghen, Annu. Rev. Nucl. Part. Sci. **57**, 171 (2007).

[36] D. Borisyuk and A. Kobushkin, Phys. Rev. C **74**, 065203 (2006).

[37] D. Borisyuk and A. Kobushkin, Phys. Rev. C **78**, 025208 (2008).

[38] D. Borisyuk and A. Kobushkin, Phys. Rev. C **83**, 025203 (2011).

[39] M. Gorchtein, Phys. Lett. B **644**, 322 (2007).

[40] E. A. Kuraev and E. Tomasi-Gustafsson, Phys. Part. Nucl. Lett. **7**, 67 (2010).

[41] M. A. Belushkin, H. W. Hammer, and U.-G. Meißner, Phys. Rev. C **75**, 035202 (2007).

[42] M. A. Belushkin, H. W. Hammer, and U.-G. Meißner, Phys. Lett. B **658**, 138 (2008).

[43] I. T. Lorenz, H. W. Hammer, and U.-G. Meißner, Eur. Phys. J. A **48**, 151 (2012).

[44] M. Hoferichter, B. Kubis, J. Ruiz de Elvira, H.-W. Hammer, and U.-G. Meißner, Eur. Phys. J. A **52**, 331 (2016).

[45] O. Tomalak and M. Vanderhaeghen, Eur. Phys. J. A **51**, 24 (2015).

[46] O. Tomalak and M. Vanderhaeghen, Phys. Rev. D **93**, 013023 (2016).

[47] O. Tomalak and M. Vanderhaeghen, Eur. Phys. J. C **76**, 125 (2016).

[48] O. Tomalak and M. Vanderhaeghen, Eur. Phys. J. C **78**, 514 (2018).

[49] O. Tomalak, Eur. Phys. J. C **77**, 858 (2017).

[50] S. Kondratyuk and O. Scholten, Phys. Rev. C **64**, 024005 (2001).

[51] G. Penner and U. Mosel, Phys. Rev. C **66**, 055212 (2002).

[52] A. Y. Korchin and O. Scholten, Phys. Rev. C **68**, 045206 (2003).

[53] S. Kondratyuk, P. G. Blunden, W. Melnitchouk, and J. A. Tjon, Phys. Rev. Lett. **95**, 172503 (2005).

[54] S. Kondratyuk and P. G. Blunden, Phys. Rev. C **75**, 038201 (2007).

[55] H. Q. Zhou, C. Wen Kao, S. N. Yang, and K. Nagata, Phys. Rev. C **81**, 035208 (2010).

[56] P. G. Blunden, W. Melnitchouk, and J. A. Tjon, Phys. Rev. Lett. **91**, 142304 (2003).

[57] O. Koshchii and A. Afanasev, Phys. Rev. D **96**, 016005 (2017).

[58] V. Bernard, N. Kaiser, and U.-G. Meißner, Int. J. Mod. Phys. E **04**, 193 (1995).

[59] V. Bernard, Prog. Part. Nucl. Phys. **60**, 82 (2008).

[60] P. Talukdar *et al.* (to be published).

[61] I. Sick and D. Trautmann, Nucl. Phys. **A637**, 559 (1998).

[62] P. G. Blunden and I. Sick, Phys. Rev. C **72**, 057601 (2005).

[63] G. 't Hooft and M. Veltman, Nucl. Phys. **B153**, 365 (1979).

[64] G. Passarino and M. Veltman, Nucl. Phys. **B160**, 151 (1979).

[65] M. Beneke and V. A. Smirnov, Nucl. Phys. **B522**, 321 (1998).

[66] A. I. Davydychev and A. G. Grozin, Eur. Phys. J. C **20**, 333 (2001).

[67] J. Zupan, Eur. Phys. J. C **25**, 233 (2002).